Innovative Infrastructure Solutions (2019) 4:37
https://doi.org/10.1007/s41062-019-0223-2

TECHNICAL NOTE

Finite element-based probabilistic stability analysis of rock-fill tailing dam considering regional seismicity

A. Hegde[1] · **Tanmoy Das**[1]

Received: 20 March 2019 / Accepted: 13 May 2019 / Published online: 16 May 2019

Abstract

The recent tailing dam failure in Brazil has again emphasized the need of performing robust stability analysis prior to construction. This paper demonstrates the probabilistic dynamic stability analysis of tailing dams considering an existing rock-fill tailing dam in India. The stability analysis was performed using 2D finite element-based package RS^2. In the probabilistic analysis, the strength parameters such as cohesion (c) and the friction angle (φ) were considered as random variables. In total, 3000 numbers of samples were generated assuming a normal distribution. Monte Carlo simulation was used to evaluate the probability of failure (PoF) and reliability index. Strength reduction method was used for the finite element analyses. A pseudo-static seismic loading was incorporated in the strength reduction analysis to check the seismic stability of the dam. A factor of safety (FoS) of 1.15 was observed from the deterministic analysis for downstream slope. For the same case, the probabilistic analysis provided a mean FoS of 1.19 with 5.46% probability of failure. The FoS values and the locations of the critical failure surface obtained by the limit equilibrium method and finite element method were compared. The observed FoS values were found to be higher than the values specified in the IS 7894-1975 (reaffirmed in 1997) and ANCOLD (1999). In the case of pseudo-static approach, the maximum displacement of 0.53 m was observed in the slope. Furthermore, nonlinear dynamic stability analysis was performed to simulate a true earthquake event. The permanent deformation of the slope after the earthquake was found to be 0.40 m. The zone of failure observed in both pseudo-static and nonlinear dynamic stability analyses was found to be the same. Overall, the results revealed that the spatial variability of the soil significantly influences the FoS values.

Keywords Tailing dam · Random variable · Monte Carlo simulation · Strength reduction method · Spatial variability

List of symbols

c	Cohesion (KPA)
c_f	Factored cohesion (kPa)
CoVs	Coefficient of variation in normal random variables (dimensionless)
d	Standard normal deviate (dimensionless)
E	Young's modulus (MPa)
E_s	Spatial element size (m)
$f_{\max}$	Maximum frequency (Hz)
$f(s)$	Probability density function of normal random variables (dimensionless)
G	Shear modulus of soil (GPa)
n	Number of random variables (dimensionless)
Ns	Number of sample having critical SRF less than or equal to 1 (dimensionless)
N_{total}	Total number of sample (dimensionless)
PoF	Probability of failure (%)
$R_{\min}$	Minimum number of realization (dimensionless)
RI	Reliability index (dimensionless)
s	Normal random variable (dimensionless)
SRF	Strength reduction factor (dimensionless)
Vs	Shear wave speed (m/s)
α_M	Rayleigh alpha constant (s^{-1})
β_K	Rayleigh beta constant (s)
γ	Unit weight of soil (kN/m^3)
ε	Relative percentage error in estimating probability of failure (%)
ζ_i	Damping ratio for mode i (%)
λ	Wave length associated with the highest frequency component (m)
μ_s	Mean of normal random variables (dimensionless)

✉ A. Hegde
ahegde@iitp.ac.in

Tanmoy Das
tanmoy.mtce17@iitp.ac.in

[1] Department of Civil and Environmental Engineering, Indian Institute of Technology Patna, Patna 801106, India

μ_{SRF} Mean of critical SRF values (dimensionless)
ν Poisson's ratio (dimensionless)
ρ Bulk unit weight of soil (kN/m^3)
σ_n Normal stress in soil (kN/m^2)
σ_s Standard deviation of normal random variables (dimensionless)
σ_{SRF} Standard deviation of critical SRF values (dimensionless)
τ_f Shear stress in soil on the sliding surface (kN/m^2)
φ Friction angle (°)
φ_f Factored friction angle (°)
ω_i Natural frequency of mode i (rad/s)

Introduction

Mining operations around the world generate a vast amount of waste products as a result of ore extraction and its refining processes. The waste materials remaining after ore dressing processes are usually collected in the form of a slurry. These slurry wastes are technically termed as tailings and retained in specially designed dams to diminish its adverse effects on the environment. Failure of the tailing dams may lead to loss of lives and extensive damage of assets together with long-term pollution in downstream areas. Therefore, it is essential to ensure the stability of the tailing dam for the safety of the downstream locality. As per the database of the International Commission on Large Dams (ICOLD) [1] and the United Nations Environment Programme (UNEP) [2], more than a few hundreds of tailing dams have failed in the past. Rico et al. [3] reported 147 failure cases of tailing dam across Europe and the USA. Most recently, Brazil has witnessed one of the worst tailing dam collapses, causing the environmental catastrophe in the country. Over the years, the safety of tailing dams has become the prime concern of geotechnical engineers. As per the United States Committee on Large Dams (USCOLD) [4] and UNEP [2] data, most of the tailing dam failures are due to slope instability.

In general, stability analyses are carried out by conventional deterministic methods with a single factor of safety (FoS). Unfortunately, deterministic methods do not account for the uncertainty involved in soil properties in an explicit manner. Uncertainty in slope stability analysis originates mainly due to soil inherent spatial variability. Apart from spatial variability, design approximations, assumptions, measurement errors, absence of geological data, etc. would make geotechnical designs more uncertain. El-Ramly [5] stated that probabilistic analyses allow uncertainty to be quantified and incorporated rationally into the design process. Effective application of the probabilistic concept in slope stability analysis was started using first-order second moment method [6–11]. Over the last three decades, the concepts and principles of probabilistic slope stability analysis have been further developed. Of late, the probabilistic stability analysis using Monte Carlo simulation (MCS) has been extensively used by many researchers [8, 12–15]. Most of these previous studies have used the limit equilibrium method (LEM). An important drawback of the LEM method is that the stress–strain relation of soil is not considered in the analysis. Besides that, several assumptions are required to calculate the FoS. Furthermore, the complex cases cannot be studied with precision using LEM. In the recent past, FEM has been increasingly used as an alternative of LEM in slope stability-related studies [16–21]. Generally, the strength reduction method (SRM) is used for slope stability analysis in FEM. This method was first introduced by Zienkiewicz et al. [22]. Later on, many researchers adopted this method to analyze the slope stability [17, 18, 23–25]. In SRM, it is not essential to divide the domain into vertical slices. Hence, no assumptions are required about the slip surface. The FoS is calculated by repeated nonlinear calculations by progressively reducing strength parameters until the failure of the slope. However, the cases of finite element slope stability analysis in the probabilistic framework are very limited.

The present study highlights the probabilistic stability analysis results of an existing tailing dam using FEM. The FEM results are also compared with the traditional LEM. The seismic stability of the dam section has been evaluated considering the pseudo-static approach in the first part of the paper. In the second part, a dynamic finite element analysis considering a true earthquake event has been performed to determine the post-earthquake deformation.

Stability analysis based on the pseudo-static approach

Methodology

The geometry of a tailing dam reported by Sitharam and Hegde [26] was considered in the analyses. The reported tailing dam is located in the northern part of India in Rajasthan. The height of the dam section is 51 m. The dam was constructed on the low permeability soil underlain by rocky strata. The depth of the overburden soil varies from 1 to 3 m in the vicinity. The layer of weathered rock below the soil overburden is existing up to a depth of 10 m. Beyond 10 m, a hard layer of granitic gneiss exists. Sitharam and Hegde [26] reported that, due to low permeability, the top clayey soil behaves like aquicludes. A conceptual sketch of the dam section is shown in Fig. 1.

The dam section was modeled as a two-dimensional plane strain problem. FEM-based commercial program RS^2 was used to perform the analyses. To determine the FoS using FEM, the strength reduction technique was adopted. This

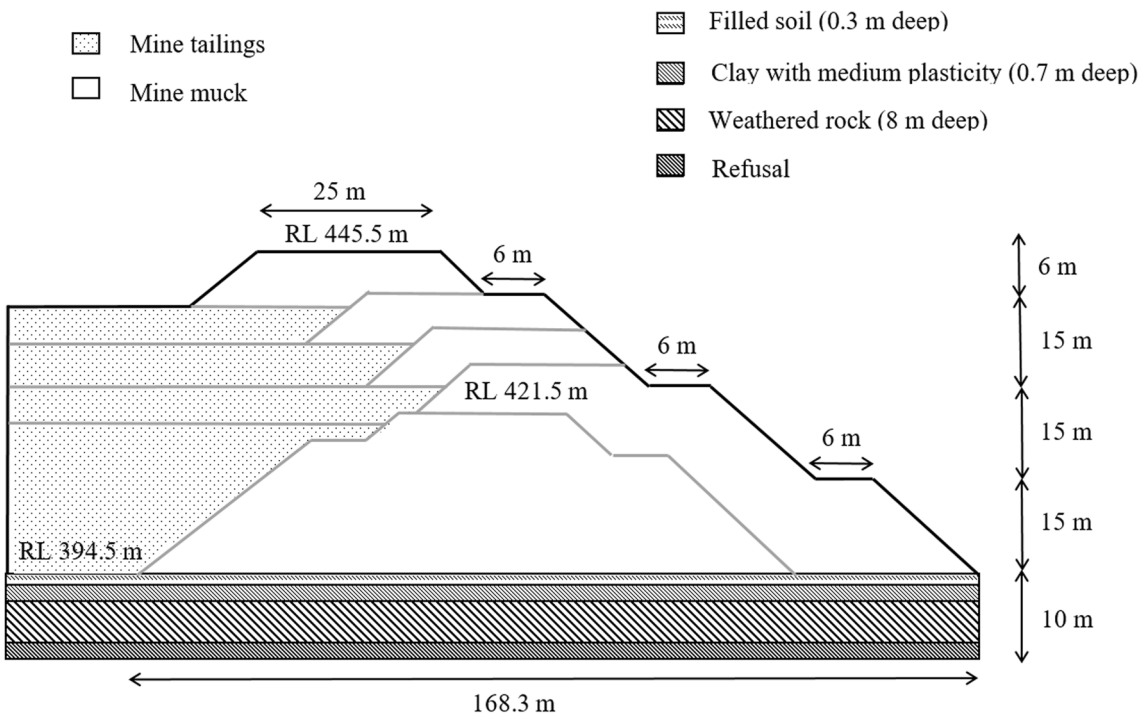

Fig. 1 Conceptual sketch of the tailing dam section (modified from Sitharam and Hegde [26])

technique gradually reduces the strength parameters by a factor known as the strength reduction factor (SRF) until failure of the slope occurs. The minimum SRF at which the failure occurs is termed as critical strength reduction factor. The critical SRF is similar to FoS in LEM. Duncan [27] stated that, like the FoS, SRF is the factor by which the shear strength must be divided so that the reduced strength is in barely stable equilibrium with the shear stress. The shear stress on the sliding surface (τ_f) can be calculated as:

$$\tau_f = c_f + \sigma_n \tan\varphi_f \tag{1}$$

where σ_n is the normal is stress and c_f and φ_f are the factored shear strength parameters. These shear strength parameters are defined as:

$$c_f = \frac{c}{\text{SRF}} \tag{2}$$

$$\varphi_f = \tan^{-1}\left(\frac{\tan\varphi}{\text{SRF}}\right) \tag{3}$$

In the analysis, Mohr–Coulomb yield criteria were used to simulate the soil materials. The non-varying soil properties considered in the analyses are presented in Table 1. In the deterministic analysis, the mean value of the variables was considered. Gravity analysis was executed with the actual ground surface so that the stresses are allowed to reach equilibrium state under self-weight. The slope model was discretized uniformly using 3000 numbers of elements.

Table 1 Constant soil parameters used for deterministic analysis

Constant properties	Mine muck	Mine tailings
Unit weight (γ) (kN/m^3)	20.7	20
Poisson's ratio (υ)	0.29	0.29
Young's modulus (E) (MPa)	25.7	12.8

A sensitivity analysis was performed to understand the effect of different element types on the accuracy of the results. Based on the sensitivity analysis, six-noded triangular mesh was used for model discretization. The discretized model is shown in Fig. 2. Appropriate boundary conditions were applied using pins at the bottom and rollers at the side to allow vertical deformations (Table 2).

Generally, FoS of earthen dams is evaluated against three major conditions, namely end of construction, sudden drawdown and steady seepage. In the present case, the tailing dam was constructed using waste rocks generated during the mining process. Hence, the possibility of pore water pressure generation is negligible. Sitharam and Hegde [14] reported that the drawdown situation does not occur in this particular tailing dam. The upstream face of the dam was covered with an impervious clay liner. Hence, the steady seepage situation also does not arise. Only the end of construction with and without earthquake conditions becomes critical. Hence, the FoS against the end of construction with earthquake condition was analyzed in this study. The tailing dam is located

in the earthquake zone-II as per seismic zonal divisions in India as per IS 1893 [28]. The value of the horizontal seismic coefficient equal to 0.06 was considered. Due to the presence of rocky strata, it is evident that the failure surface would only pass through the face or the toe of the dam.

Variability and uncertainty were quantified by treating soil parameters as the random variables. A large range of soil parameter values was generated as defined by its probability density function (PDF). Most common PDF used for defining soil strength parameters is either normal distribution or lognormal distribution. Lumb [29] demonstrated that normal distributions are suitable for parameters like effective cohesion and friction angle. The applicability of normal distribution for soil properties was also supported by Lee et al. [30]. In the probabilistic analysis, soil strength parameters, c, and φ were characterized statistically by a normal distribution with the specified mean (μ_s) and standard deviation (σ_s). All the statistical properties of variables are shown in Table 3. The probability density function for the random variable following normal distribution is given by:

$$f(s) = \frac{1}{\sigma_s\sqrt{2\pi}}\exp\left[-\frac{1}{2}\left(\frac{s-\mu_s}{\sigma_s}\right)^2\right] \quad (4)$$

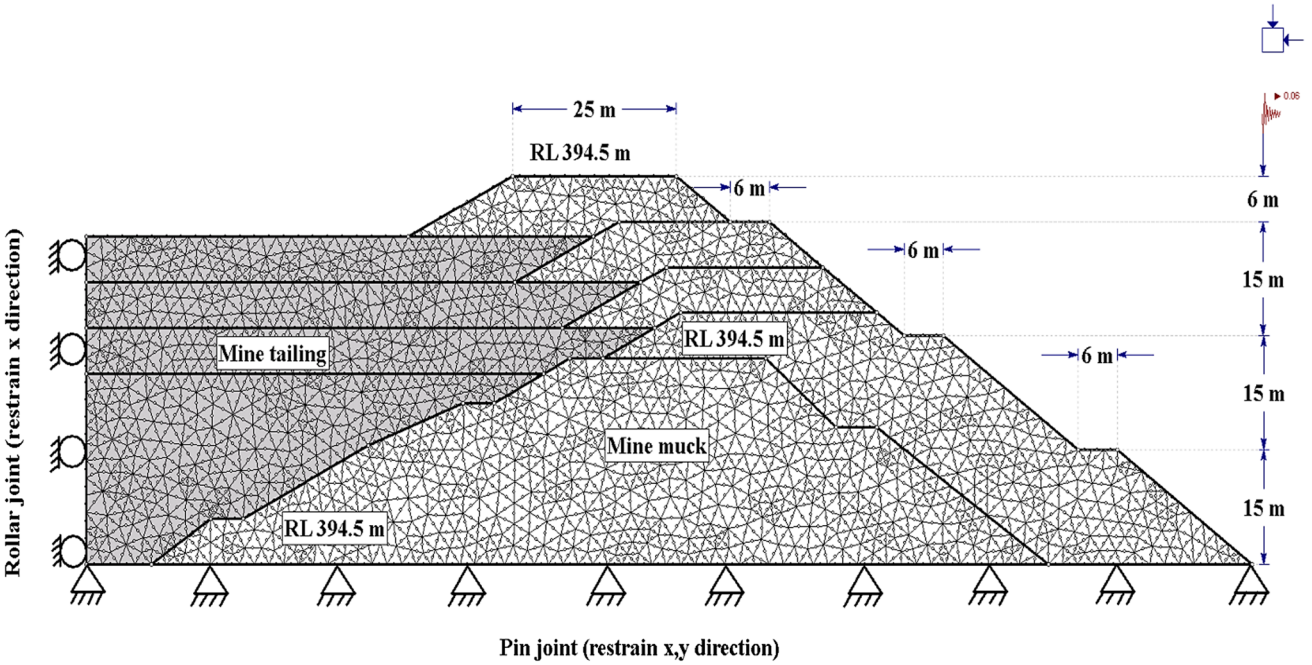

Fig. 2 Meshed model with boundary conditions

Table 2 Statistical properties of soil parameters used in the probabilistic analysis [14]

Material	Property		Distribution	Mean	Min	Max	SD	Coefficient of variation (%)
Mine muck	(a)	Cohesion, c (kPa)	Normal	2	0	4	1	50
	(b)	Friction angle, φ (degree)	Normal	39	30	48	3	7.69
Mine tailings	(c)	Cohesion, c (kPa)	Normal	1	0	2	1	100
	(d)	Friction angle, φ (degree)	Normal	35	26	44	3	8.57

Table 3 Probabilistic outputs for different methods

Outputs		Ordinary	Bishop	Spencer	Janbu	Morgenstern–Price	SRM
Probability of failure	Circular failure surface	9.73	6.5	6.77	9.9	6.7	5.46
	Non-circular failure surface	7.97	5.97	7.8	10.93	8.4	
Reliability index	Circular failure surface	1.30	1.50	1.48	1.29	1.4	1.6

where s is the normal random variable. The typical normal distributions of mine muck friction angle (φ) and cohesion (c) are shown in Fig. 3a, b. Variability in soil properties is often expressed in terms of the ratio between standard deviation and mean, named as the coefficient of variation:

$$\text{CoVs} = \frac{\sigma_s}{\mu_s} \tag{5}$$

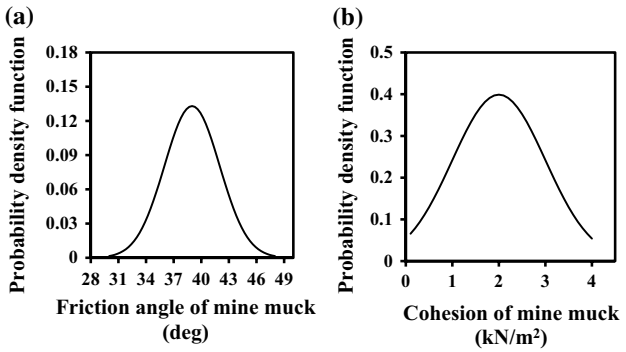

Fig. 3 Typical normal distribution of variables used in the analysis: **a** mine muck friction angle; **b** mine muck cohesion

Another way to calculate the statistical parameters (e.g., mean, standard deviation) of the performance function is to use of Monte Carlo simulation (MCS) method. MCS is generally used to model the probability of different outcomes in a process that cannot easily be predicted due to the intervention of random variables and uncertainty. This method generates a set of random variables from a given input PDF. Based on those random variables, the performance functions are evaluated for each set. Figure 4 schematically illustrates the methodology used to evaluate the PoF and the reliability of slope using MCS. Since MCS is an approximate method, its accuracy essentially depends on the number of iterations. Hence, it is important to determine the minimum number of realizations required to produce a reliable and accurate result. On the other hand, repetitive finite element analysis with a different number of realization is very time-consuming. Hahn and Shapiro [31] suggested that the minimum number of realization is a function of the number of random variables and desired confidence level. The minimum number of realizations (R_{min}) required for MCS is determined as:

$$R_{\text{min}} = n\left(\frac{100d}{\varepsilon}\right)^2 \frac{(1-\text{PoF})}{\text{PoF}} \tag{6}$$

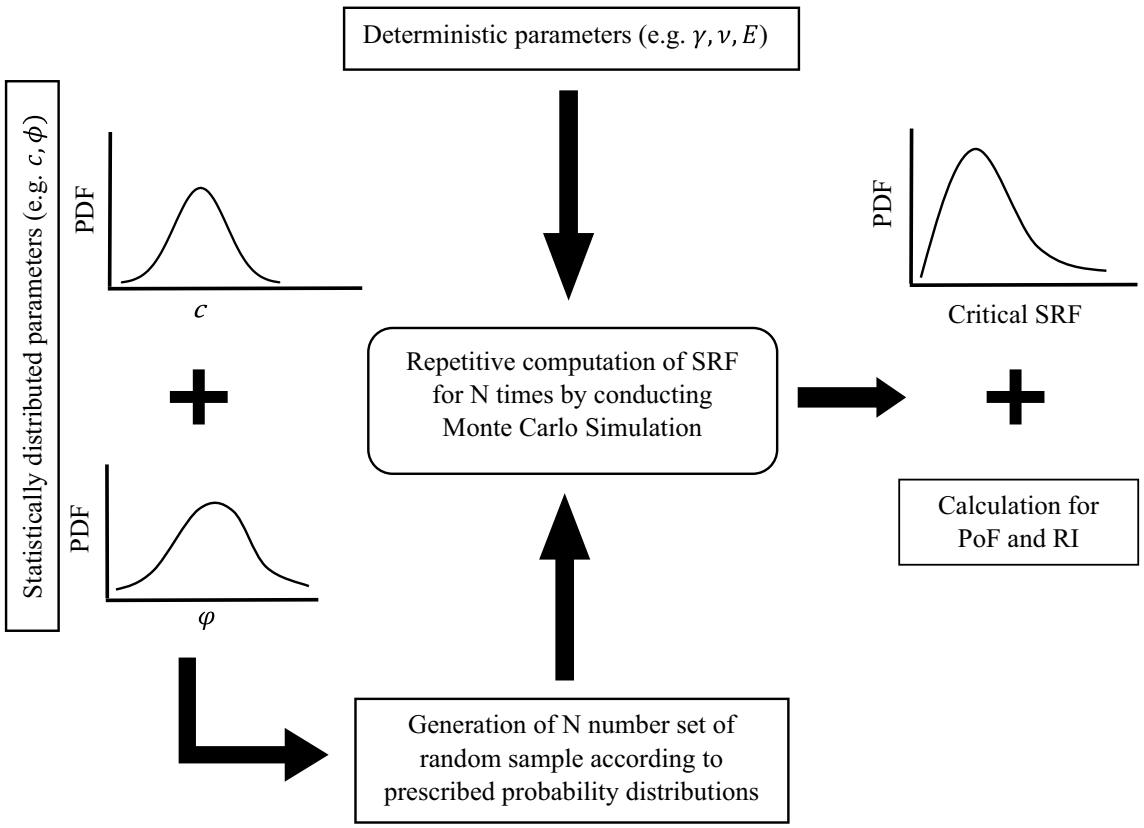

Fig. 4 Schematic representation of methodology used for probabilistic analysis

where n is number of random variables; ϵ is relative percentage error in estimating PoF; and d is standard normal deviate according to the desired confidence levels. Chok [32] stated that, in order to achieve a relative percentage error less than 5% or for a 95% confidence level with two random variables problem, the minimum number of realizations must be 3000 or more. Hence, in this study, 3000 numbers of realizations were adopted. The samples were generated as per the prescribed probability distribution. For each sample, deterministic analysis was performed using MCS. Hence, for a total of 3000 samples, the same numbers of critical SRF were obtained. Then, the system probability of failure was calculated using the following equation:

$$\mathrm{PoF} = \frac{Ns}{N_{\mathrm{total}}} \tag{7}$$

where Ns is the number of sample having critical SRF less than or equal to 1 and N_{total} is the total number of samples. Similarly, reliability index can be calculated as:

$$\mathrm{RI} = \frac{\mu_{\mathrm{SRF}} - 1}{\sigma_{\mathrm{SRF}}} \tag{8}$$

where μ_{SRF} is the mean of critical SRF values and σ_{SRF} is the standard deviation of critical SRF values.

Validation

Initially, the FEM model was validated with LEM results reported by Sitharam and Hegde [26] for the same dam section. The cross section and the material properties similar to Sitharam and Hegde [26] were used for the analyses. Figure 5a, b shows the results of the deterministic analysis performed by Sitharam and Hegde [26] and the present study, respectively. Figure 5b demonstrates the accumulation and localization of stresses near the crest causing the failure. A FoS value of 1.15 in terms of critical SRF was obtained from deterministic analysis in FEM. The obtained FoS value was found to be in good agreement with the value reported by Sitharam and Hegde [26]. Once the validation is completed, the same cross section was used for probabilistic analysis.

Results and discussions

In FEM, all the FoS values were calculated in terms of critical SRF. Figure 6 shows the results of the probabilistic analysis performed using SRM. A mean FoS of 1.19 and PoF of 5.46% were observed. The RI of the slope was found to be 1.6 for the slope. The vulnerable region was identified below the crest. The probabilistic analysis results obtained from FEM were compared with the LEM. The PoF and RI were calculated assuming both circular and non-circular failure surfaces in the LEM. The slip surfaces obtained from five popular limit equilibrium methods, namely ordinary, Bishop's, Janbu's, Spencer's and Morgenstern–Price, were compared with SRM. Figure 7 shows the probabilistic analysis results of LEM assuming circular failure surface. In the case of circular failure surface, the location of the slip surface was found same for all the limit equilibrium methods. The FoS values and critical failure surfaces determined by the FEM and LEM were found to be similar. Figure 8 shows the location of generated slip surfaces assuming non-circular failure surface. The failure zone obtained from Ordinary and Janbu's method was different from that obtained from the SRM. On the other hand, the failure zone obtained from other three limit equilibrium methods was similar to SRM. The FoS associated with non-circular failure surface was found to be 1.15 using Bishop's, Spencer's and Morgenstern–Price method. The observed FoS value was found to be same as that obtained from SRM. However, FoS values obtained by ordinary and Janbu's methods were slightly varied from the SRM obtained values.

Table 3 highlights the probabilistic outputs of FEM and LEM with different failure surface conditions. It was observed that FEM provides a lesser value of PoF as compared to the limit equilibrium method. Slight variation in the calculated values was observed in different limit equilibrium methods. It was due to the different assumptions involved in the different limit equilibrium methods about failure surface. On the other hand, without any assumption, FEM provides an acceptable result. In overall, FEM and LEM results were found to be in good agreement with each other. The calculated FoS values were found higher than the threshold value suggested by IS 7894 [33] and ANCOLD [34] as listed in Table 4. Likewise, Dell'Avanzi and Sayão [35] provided the acceptable limit of PoF in different types of geotechnical structures as shown in Table 5. The calculated PoF values of the tailing dam were found within the tolerable limit.

Figure 9 shows the deformation vectors obtained from FEM. It indicates an outward and downward movement of soil material. The deformed mesh clearly shows that the materials are moving outward from the parent mass, majorly near the crest of the dam. Hence, the crest part of the slope was found highly susceptible to failure. Figure 10a shows the maximum displacement obtained for different values of SRF. With the increase in SRF, the strength properties decreased, leading to the increment in maximum displacement. Beyond SRF of 1.15, there was a big jump in the displacement indicating the failure. Hence, SRF of 1.15 was considered as critical SRF. In Fig. 10b, a comparison of the displacement variations along the free slope boundary has been portrayed between the deterministic and probabilistic analyses. The displacement at 20 different points from crest to toe along the free boundary was plotted for critical SRF 1.15. It was observed that the displacement obtained from

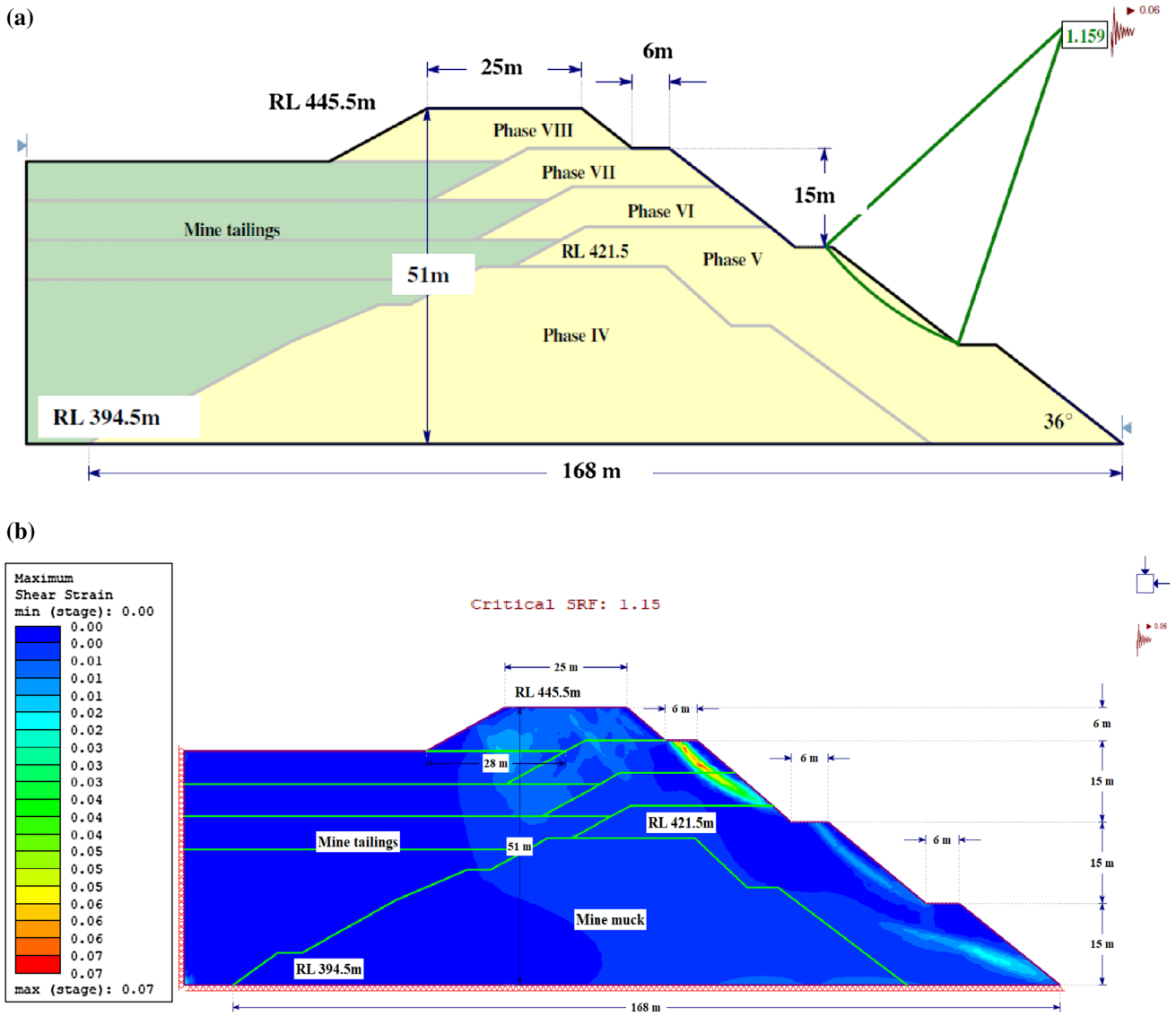

Fig. 5 Comparison of the results: **a** LEM results of Sitharam and Hegde [26]; **b** FEM results of the present study

the probabilistic analysis is slightly higher than that from the deterministic analysis. The maximum displacement of 0.53 m was calculated under pseudo-static seismic loading with a horizontal seismic coefficient of 0.06. The obtained displacement was found to be within the tolerable limit suggested by various researchers [36–38].

The inherent variability in the measured data can be portrayed graphically in the form of a histogram [39]. The frequency histogram of the generated critical SRF values (i.e., deterministic FoS values) using 3000 Monte Carlo sampling is shown in Fig. 11a. From this figure, the PoF can also be determined. Here, the PoF is equal to the area of the histogram having the critical SRF less than 1, divided by the total area of the histogram. To check the validity of the distributional assumption for the output variable, the q–q (quantile–quantile) plot was plotted. The q–q plot was plotted by sorting the sample data in ascending order. The sorted data were plotted against quantile calculated from a theoretical distribution. If a variable is normally distributed, the normal quantile plot approximates a diagonal straight line. Figure 11b represents a normal quantile plot of all the critical SRF values generated using MCS. The generated critical SRF values were found to be normally distributed as all the points on the graph follow a sloped straight path. In this way, the distribution of the output parameter was same as that of the distribution of the input parameter, indicating the accuracy of the analysis.

Furthermore, if two variables are involved, the joint variability may be portrayed in a scattergram [39]. Also, a suitable relationship between two variables can be established

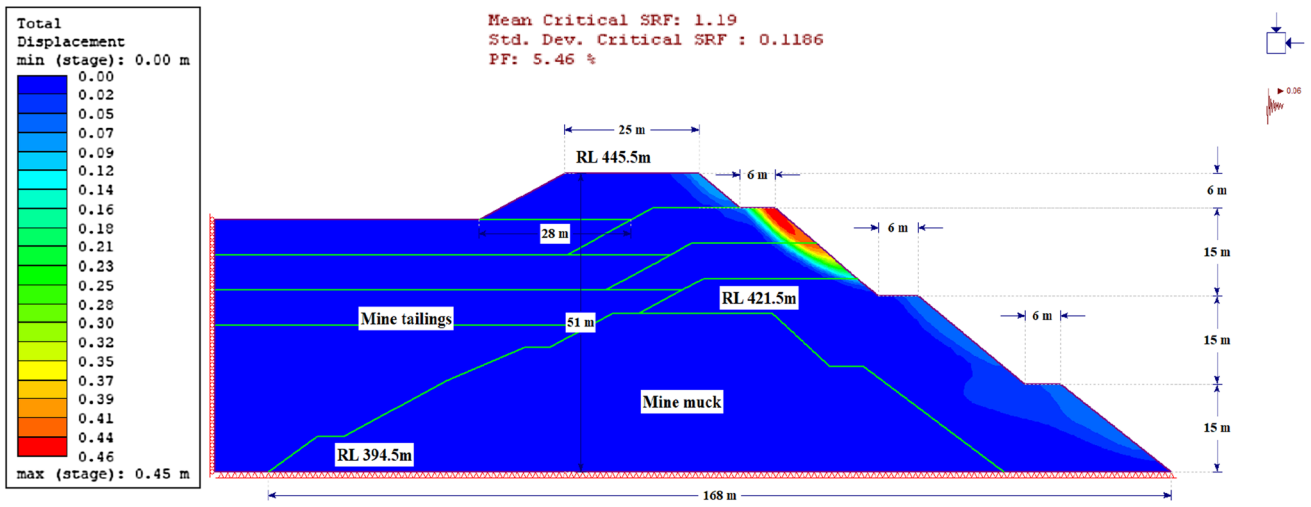

Fig. 6 Displacement contour showing the vulnerable region

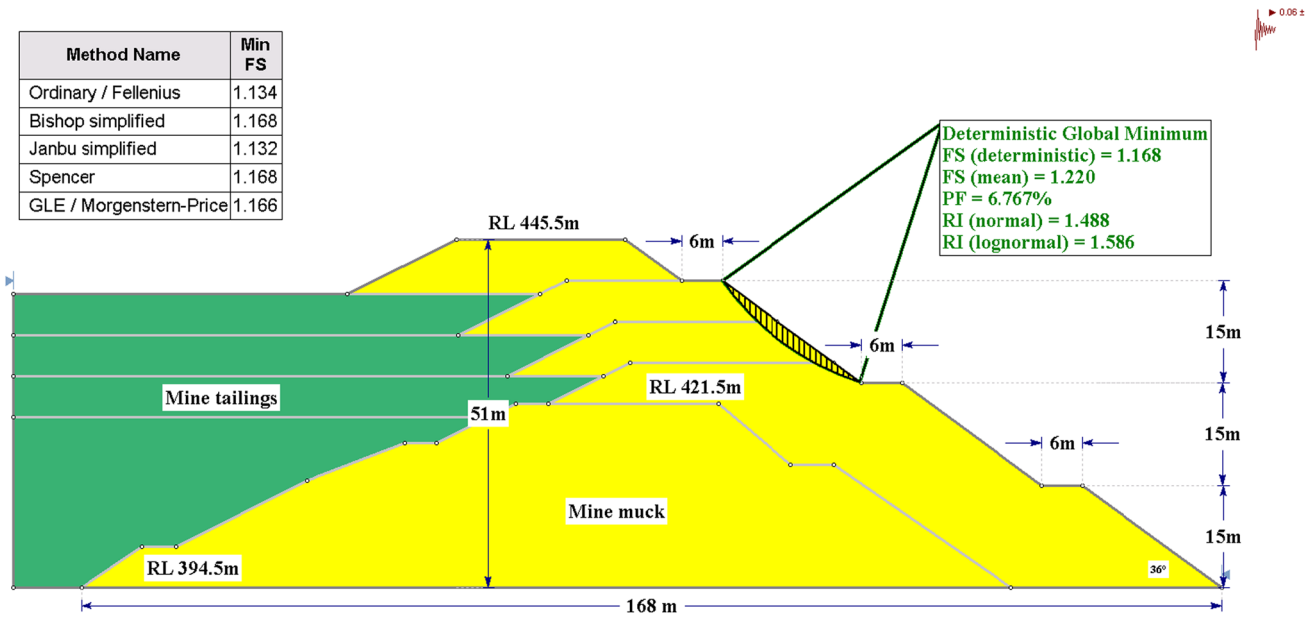

Fig. 7 Result of probabilistic analysis using LEM for circular failure surface

using scattergram. Figure 12 represents the scattergrams plotted between the output parameter and two input variables, namely friction angle and cohesion of the mine muck. The plot between the critical SRF and friction angle of mine muck shows a strong correlation, as all the points on the plot are converging toward the regression line. On the other hand, a negligible correlation was observed between mine muck cohesion values and generated critical SRF values. To measure the correlation, coefficient of correlation was calculated between two variables. A strong correlation was observed between critical SRF values and friction angle with a coefficient of correlation of 0.97. On the other hand, less dependency of critical SRF on the cohesion was observed as the magnitude of the correlation coefficient is 0.02. It indicates that the friction angle has a strong influence on the FoS values and PoF.

Dynamic slope stability analysis

To simulate the deformation of the slope during a real earthquake event, the dynamic slope stability analysis was performed in FEM. The acceleration time history of a past earthquake of the particular region was taken into consideration. Figure 13a shows the acceleration time history graph of the

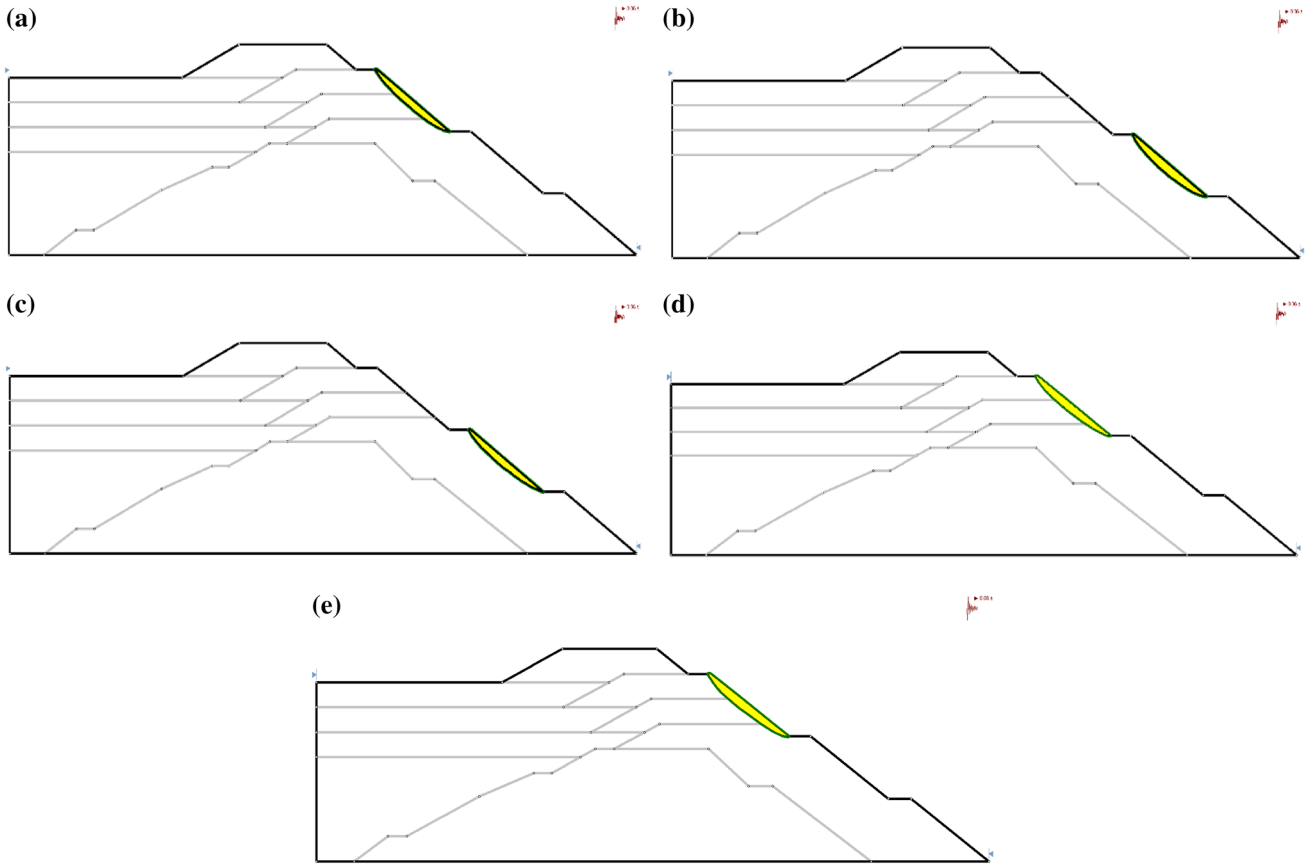

Fig. 8 Slip surfaces obtained from different LEM methods using non-circular failure surface: **a** Bishop's; **b** Janbu's; **c** ordinary; **d** Spencer's; **e** Morgenstern–Price

Table 4 Minimum desired values of a factor of safety for different loading conditions as per IS 7894 [33]

Case no.	Loading condition of the dam	Slope most likely to be critical	Minimum desired factor of safety
I.	Construction condition with or without partial pool	Upstream and downstream	1
II.	Reservoir partial pool	Upstream	1.3
III.	Sudden drawdown:		
	(a) Maximum head water to minimum with tail water at maximum	Upstream	1.3
	(b) Maximum tail water to minimum with reservoir full	Downstream	1.3
IV.	Steady seepage with reservoir full	Downstream	1.5
V.	Steady seepage with sustained rainfall	Downstream	1.3
VI.	Earthquake condition:		
	(a) Steady seepage	Downstream	1
	(b) Reservoir full	Upstream	1

2006 Alwar earthquake. Alwar is located in the northeastern part of Rajasthan. The earthquake has a dominant effect across the width of the dam section. Hence, a plane strain analysis was performed. The mesh size and material properties were kept the same as pseudo-static strength reduction analysis. The design earthquake ground motions are usually provided as outcrop motions. Therefore, it is necessary to deconvolute the given time history data. Deconvolution is a filtering process which removes a wavelet from the recorded seismic trace by reversing the process of convolution. The objective of deconvolution is to extract the reflectivity function from the seismic trace [40]. To deconvolute the earthquake data,

Table 5 Acceptable probability of failure in different types of geotechnical structures [35]

Case	Reliability index	Probability of failure (%)
Foundations	2.3–3.0	$1–10^{-1}$
Mining slopes	1.0–2.3	$10–10^{-1}$
Dams	3.5–5.0	$10^{-1}–10^{-3}$
Retaining structures	2.0–3.0	$10^{-1}–10^{-1}$

initially acceleration time history was applied at the top of the model and the resultant velocity time history was plotted. Half of the calculated velocity was applied to the base of the model. The top of the model is a free surface with zero shear stress, and hence, the upward and downward waves at the top of the model must be equal. Hence, the velocity history applied at the base of the model must be one half of the given outcrop motion. It was observed that the velocity history applied at top of the model was found to be identical to that obtained at the bottom of the model indicating the correctness of deconvolution procedure.

While modeling the seismic condition, both the frequency content of the input wave and the wave speed of the system will affect the numerical accuracy of wave transmission. Kuhlemeyer and Lysmer [41] stated that, for the accurate representation of wave transmission through a model, the spatial element size (E_s) should be:

$$E_s \leq \frac{\lambda}{10} \tag{9}$$

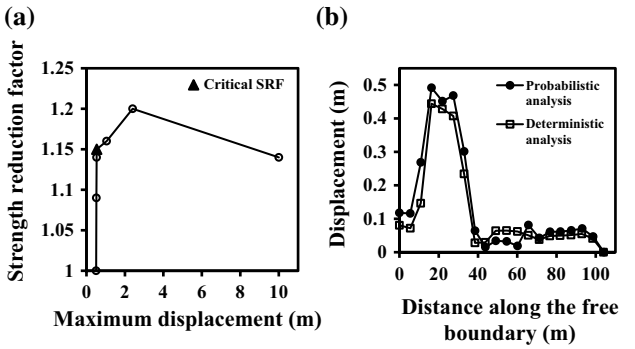

Fig. 10 Displacement profile of the dam section under pseudo-static seismic loading: **a** maximum displacement of the slope for various SRF; **b** displacement at different points from crest to toe along the free boundary of the slope

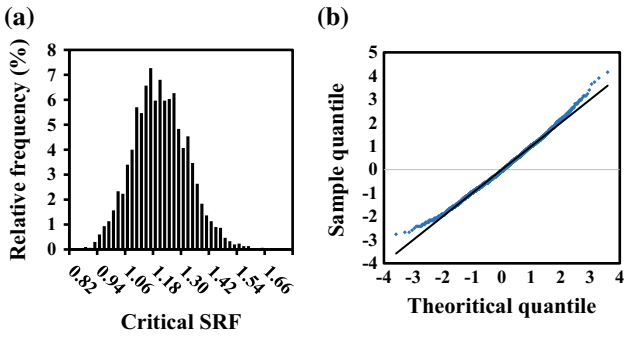

Fig. 11 Monte Carlo simulation results: **a** frequency histogram plot; **b** normal quantile plot

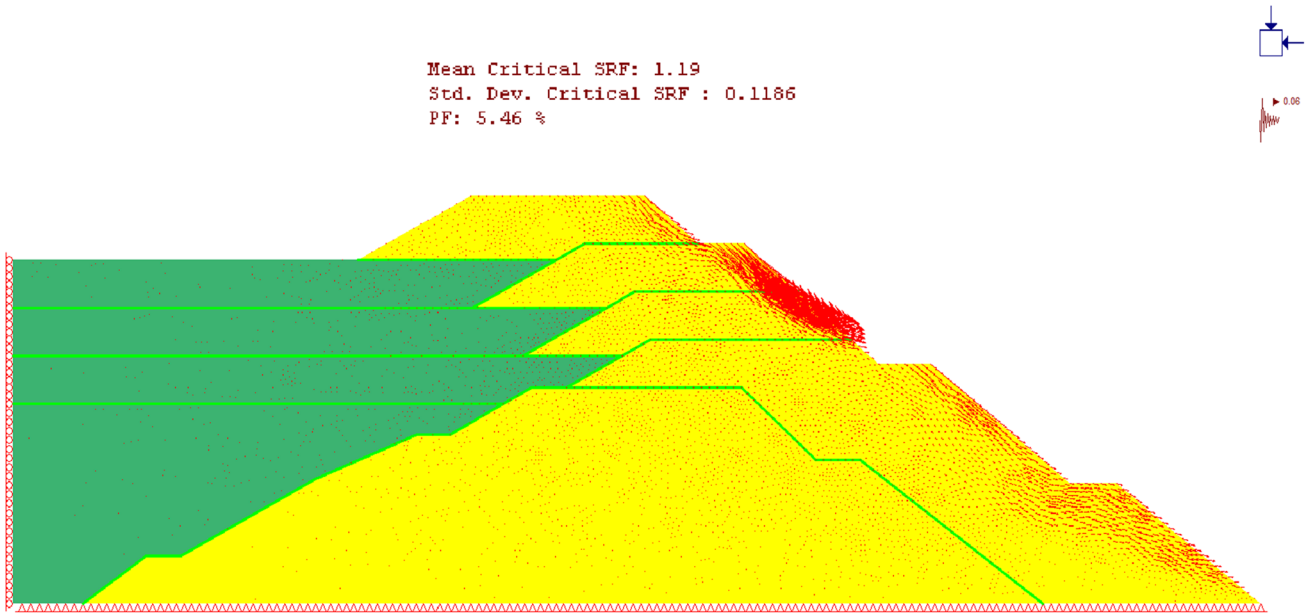

Fig. 9 Movement of the displacement vector with deformed mesh

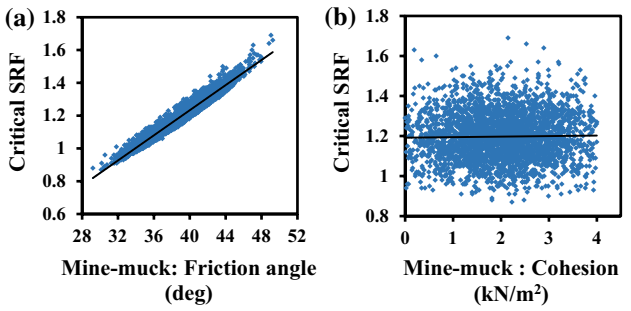

Fig. 12 Scatter plots: **a** critical SRF versus friction angle; **b** critical SRF versus cohesion

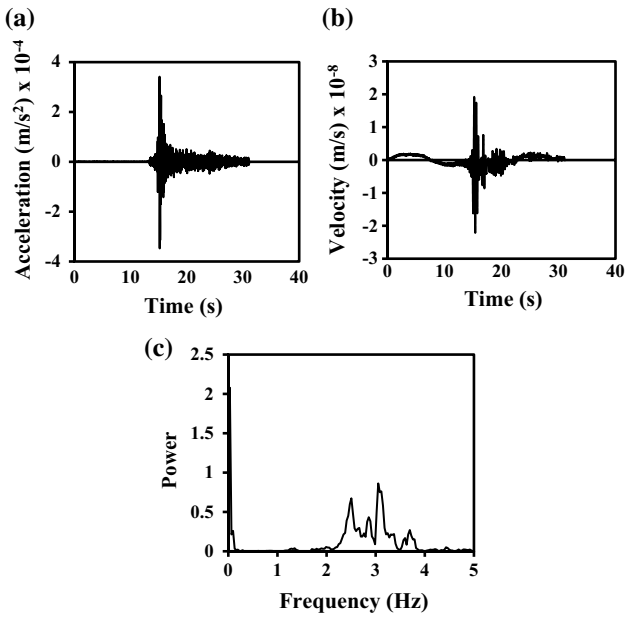

Fig. 13 Alwar Earthquake (2006): **a** acceleration time history; **b** velocity time history with filtered velocity data; **c** power versus frequency plot

where λ is the wavelength associated with the highest frequency component that contains appreciable energy. To satisfy Eq. 9, for a velocity input with high peaks and short rise time, a very fine mesh may be required. This may lead to an excessive amount of computing time. For this purpose, the input velocity was filtered and high-frequency components were removed. Figure 13b shows a velocity–time history plot with the filtered velocity data. The maximum frequency ($f_{\max}$) was calculated using the following equation:

$$f_{\max} = \frac{V_s}{\lambda} \tag{10}$$

where

$$Vs = \sqrt{\frac{G}{\rho}} \tag{11}$$

where Vs is shear wave velocity; G is shear modulus of soil; and ρ is bulk unit weight of the soil. The maximum frequency of the model was calculated as 3.5 Hz. Figure 13c demonstrates a power–frequency plot where most of the power of the earthquake occurs for frequencies of about 3.5 Hz and below. Therefore, by filtering out frequencies larger than 3.5 Hz, an accurate wave transmission through the model was obtained without losing any significant earthquake power.

The physical damping due to the viscous effects was taken into consideration via the Rayleigh damping. In this study, the appropriate damping constants for a particular damping ratio were determined for a particular mode 'i' using the following equation:

$$\zeta_i = \frac{1}{2\omega_i}\alpha_M + \frac{\omega_i}{2}\beta_K \tag{12}$$

where ζ_i is the damping ratio for mode i; ω_i is the natural frequency of mode i with unit (rad/s); α_M and β_K are constants with units of (s^{-1}) and (s), respectively. Rayleigh alpha (α_M) and beta (β_K) determine the influence of mass and stiffness in the damping of the system, respectively. To determine the appropriate Rayleigh damping values, first, the model was run as an undamped model (i.e., α_M and β_K is equal to zero) with the filtered velocity data. Then, the Rayleigh damping constants were determined so that the average damping for all the natural frequencies (from 0–3.5 Hz) is 5%. The values of two damping constants α_M and β_K were observed as 0.1 and 0.00655, respectively. Generated Rayleigh constants and filtered velocity were applied to the finite element model with appropriate dynamic boundary conditions.

Boundary condition plays a major role in the dynamic analysis. In order to avoid spurious wave reflections at the model boundary, special conditions have to be applied. In dynamic problems, fixed boundary conditions cause the reflection of outward propagating waves, effectively trapping energy inside the model [42]. Therefore, it is required to have boundary conditions that allow the necessary energy radiation. Transmitting boundary conditions are suitable for both boundary and finite element analyses, for the radiation of waves propagating in the horizontal direction [43]. Transmit boundary condition was assigned to the lateral side of the model. The bottom boundary was assigned with the absorbing boundary condition to absorb incoming shear and pressure waves traveling in the soil. The total duration of the earthquake was 31.13 s. In addition to an initial static stage, four dynamic time stages were added (5 s, 10 s, 20 s and 31.13 s) to check the deformation pattern at each stage.

Figure 14a shows the deformation contour obtained from the dynamic analysis. The crest part of the dam was found to be most vulnerable. The deformation pattern was similar to the pseudo-static seismic loading case discussed in the earlier part of the manuscript. Figure 14b shows the

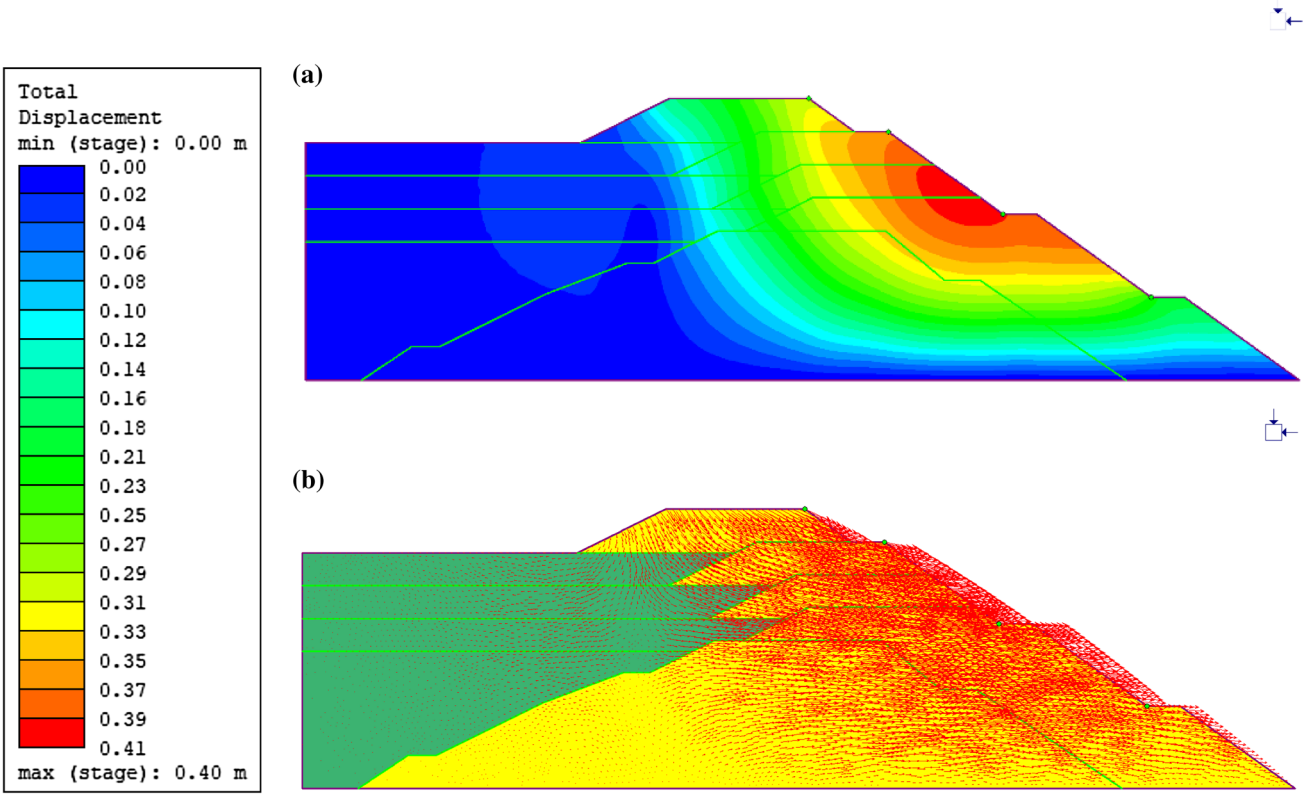

Fig. 14 Post-earthquake deformation characteristics: **a** deformation contours; **b** displacement vectors

post-earthquake displacement vectors. The movement of the soil mass was also similar to that of observed in pseudo-static approach. The horizontal displacement of the model at various time stages was graphed to record the slope movement during the seismic event. The displacement time history of the crest part is shown in Fig. 15. A maximum displacement of 0.4 m was observed at the mid-height of the tailing dam. The maximum displacement was less than that of obtained from pseudo-static strength reduction analysis.

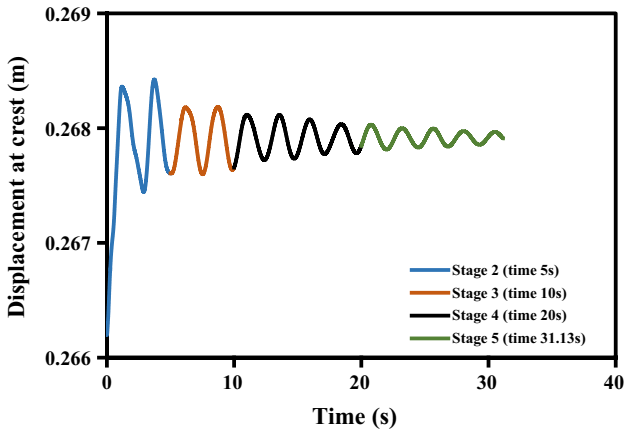

Fig. 15 Displacement time history at the crest

Conclusions

This paper proposed a FEM-based probabilistic analysis to increase the level of accuracy in tailing dam stability analysis. The section of an existing tailing dam located in northern India was considered in the analysis. The probabilistic analysis was performed considering cohesion and friction angle of the mine muck as the random variables. The FEM results were validated and compared with the LEM results. Results revealed that the spatial variability of the soil significantly influences the FoS values. The critical SRF was found to be 1.2, with good agreement with the LEM. The probabilistic analysis highlighted that the PoF in the existing condition was about 6%. Based on the results of the analyses, the friction angle of mine muck was found to be the most influencing parameter. Hence, the minor deviation in the friction angle resulted in the large variation in PoF. Further, the results of the different limit equilibrium methods were compared. Both with circular and non-circular failure surfaces were considered in the comparison. The results suggested that the Bishop's and ordinary slice methods were overestimated the PoF and RI values in the

case of non-circular failure surface as compared to the circular failure surface. The permanent deformations of 0.53 m and 0.4 m were observed in the case of pseudo-static and nonlinear dynamic analysis, respectively. The downstream displacement obtained from the probabilistic analysis was found to be higher than the deterministic analysis. However, the post-earthquake displacement pattern obtained from both the methods was similar. In overall, the probabilistic approach was found to be a robust tool to ensure all-around safety for important structures like the tailing dam.

References

1. ICOLD (2001) Tailings dams: risk of dangerous occurrences: lessons learnt from practical experiences. Bulletin (International Commission on Large Dams) p 121
2. UNEP (1996) Environmental and safety incidents concerning tailings dams at mines: results of a survey for 1980–1996. Mining Journal Research Services & United Nations Environment Programme & United Nations. Department of Humanitarian Affairs, Paris
3. Rico M, Benito G, Salgueiro AR, Díez-Herrero A, Pereira HG (2008) Reported tailings dam failures. J Hazard Mater 152:846–852
4. USCOLD Committee on Tailings Dams (1994) Tailings dam incidents. U.S. Committee on Large Dams, Denver
5. El-Ramly H, Morgenstern NR, Cruden DM (2002) Probabilistic slope stability analysis for practice. Can Geotech J 39:665–683
6. Christian JT, Ladd CC, Baecher GB (1994) Reliability applied to slope stability analysis. J Geotech Eng 120(12):2180–2207
7. Chowdhury RN, Xu DW (1995) Geotechnical system reliability of slopes. Reliability Engineering & System Safety 47(1995):141–151
8. Malkawi AIH, Hassan WF, Abdulla FA (2000) Uncertainty and reliability analysis applied to slope stability. Struct Saf 22(2000):161–187
9. Luzi L, Pergalani F, Terlien MTJ (2000) Slope vulnerability to earthquakes at subregional scale, using probabilistic techniques and geographic information systems. Eng Geol 58(2000):313–336
10. Bhattacharya G, Jana D, Ojha S, Chakraborty S (2003) Direct search for minimum reliability index of earth slopes. Comput Geotech 30(2003):455–462
11. Zhao HB (2008) Slope reliability analysis using a support vector machine. Comput Geotech 35(2008):459–467
12. Kavvadas M, Karlaftis M, Fortsakis P, Stylianidi E (2009) Probabilistic analysis in slope stability. In Proceedings of the 17th international conference on soil mechanics and geotechnical engineering, pp 1650–1653
13. Queiroz IM (2016) Comparison between deterministic and probabilistic stability analysis, featuring consequent risk assessment. International Journal of Geotechnical and Geological Engineering 10(6):636–643
14. Sitharam TG, Hegde A (2017b) Probabilistic seismic slope stability analyses of rock fill tailing dams: a case study. In Proceedings of the 19th international conference on soil mechanics and geotechnical engineering, technical committee, vol 210, pp 2439–2442
15. Sitharam TG, Hegde A (2019) A case study of probabilistic seismic slope stability analysis of rock fill tailing dam. Int J Geotech Earthq Eng 10(2):43–60
16. Zou JZ, Williams DJ, Xiong WL (1995) Search for critical slip surfaces based on finite element method. Can Geotech J 32(2):233–246
17. Griffiths DV, Lane PA (1999) Slope stability analysis by finite elements. Geotechnique 48(3):387–403
18. Zheng YR, Zhao SY, Kong WX, Deng CJ (2005) Geotechnical engineering limit analysis using finite element method. Rock Soil Mech 26(1):163–168
19. Griffiths DV, Marquez RM (2007) Three-dimensional slope stability analysis by elasto-plastic finite elements. Ge ´otechnique 57(6):537–546
20. Baba K, Bahi L, Ouadif L, Akhssas A (2012) Slope stability evaluations by limit equilibrium and finite element methods applied to a railway in the moroccan rif. Open J Civil Eng 2:27–32
21. Sharma LK, Umrao RK, Singh R, Ahmad M, Singh TN (2017) Stability investigation of hill cut soil slopes along national highway 222 at malshej ghat, maharashtra. J Geol Soc India 89:165–174
22. Zienkiewicz OC, Humpheson C, Lewis RW (1975) Associated and nonassociated visco-plasticity and plasticity in soil mechanics. Geotechnique 25(4):671–689
23. Xu B, Low BK (2006) Probabilistic stability analyses of embankments based on finite-element method. J Geotech Geoenviron Eng 132(11):1444–1454
24. Cheng YM, Lansivaara T, Wei WB (2007) Two-dimensional slope stability analysis by limit equilibrium and strength reduction methods. Comput Geotech 34(2007):137–150
25. Maji VB (2017) An insight into slope stability using strength reduction technique. J Geol Soc India 89:77–81
26. Sitharam TG, Hegde A (2017) Stability analysis of rock-fill tailing dam: an Indian case study. Int J Geotech Eng 11(4):332–342
27. Duncan JM (1996) State of the art: limit equilibrium and finite-element analysis of slopes. J Geotech Eng 122(7):577–596
28. IS 1893(I) (1984) Criteria for earthquake resistant design of the structures. Indian Standard, New Delhi
29. Lumb P (1966) The variability of natural soils. Can Geotech J 3:74–97
30. Lee IK, White W, Ingles OG (1983) Geotechnical engineering. Pitman, London
31. Hahn GJ, Shapiro SS (1967) Statistical model in engineering. Wiley, New York
32. Chok YH (2008) Modelling the effects of soil variability and vegetation on the stability of natural slopes. Doctoral thesis, The University of Adelaide, Australia
33. IS 7894 (1975) Code of practice for the stability analysis of the earth dams. Indian Standard, New Delhi
34. ANCOLD (1999) Guidelines on tailings dam design, construction and operation. Australian National Committee on Large Dam
35. Dell'Avanzi E, Sayão A (1998) Avaliação da probailidade de rupture de taludes". Congresso Brasileiro de Mecânica dos Solos e Engenharia Geotécnica 11(2):1289–1295
36. Seed HB (1979) Considerations in the earthquake-resistant design of earth and rockfill dams. In Nineteenth rankine lecture, Geotechnique, vol 29(3), pp 215–263
37. Griffrin MEH, Franklin AG (1984) Rationalizing the seismic coefficient method. Final Report, Miscellaneous Paper GL-84-13. Waterways Experiment Station, U.S. Army Corps of Engineers, Vicksburg
38. Kavazanjian EJ, Matasovic N, Hamou TH, Sabatini PJ (1997) Geotechnical engineering circular #3, Design guidance: geotechnical earthquake engineering for highways, vol 1, design principles. Federal Highway Administration, U.S. Department of Transportation, Washington
39. Ang AHS, Tang WH (2007) Probability concepts in engineering. Wiley, New Jersey

40. Arya VK, Holden HD (1978) Deconvolution of seismic data—an overview. IEEE Trans Geosci Electron 16(2):95–98
41. Kuhlemeyer RL, Lysmer J (1973) Finite element method accuracy for wave propagation problems. J Soil Mech Found Div 99(5):421–427
42. Nielsen AH (2006) Absorbing boundary conditions for seismic analysis in ABAQUS. ABAQUS Users' Conference
43. Çetin M, Mengi Y (2003) Transmitting boundary conditions suitable for analysis of dam reservoir interaction and wave load problems. Appl Math Model 27(2003):451–470